Upstream Swimming in Microbiological Flows

Arnold J. T. M. Mathijssen,[*] Tyler N. Shendruk, Julia M. Yeomans, and Amin Doostmohammadi
The Rudolf Peierls Centre for Theoretical Physics, 1 Keble Road, Oxford OX1 3NP, United Kingdom
(Received 26 March 2015; revised manuscript received 4 June 2015; published 15 January 2016)

Interactions between microorganisms and their complex flowing environments are essential in many biological systems. We develop a model for microswimmer dynamics in non-Newtonian Poiseuille flows. We predict that swimmers in shear-thickening (-thinning) fluids migrate upstream more (less) quickly than in Newtonian fluids and demonstrate that viscoelastic normal stress differences reorient swimmers causing them to migrate upstream at the centerline, in contrast to well-known boundary accumulation in quiescent Newtonian fluids. Based on these observations, we suggest a sorting mechanism to select microbes by swimming speed.

DOI: 10.1103/PhysRevLett.116.028104

Motile microorganisms ubiquitously inhabit confined and complex microenvironments. Geometrical constraints are a key regulator of rheotaxis, the reorientation of swimmers in response to external flows [1], and are essential in the design of microfluidic devices for drug delivery systems, hematology, and cytometry [2,3]. Additionally, the complexity of embedding fluids is crucial. One important aspect of the complexity arises from the dual fluidic and elastic (viscoelastic) behavior of many biological fluids, such as mucus and extracellular matrix gels [4–6] or blood at macroscopic length scales [7–9].

Important correlations have been found between non-Newtonian behavior of the fluid and pathological phenomena. Gastric mucus viscoelasticity effects swimming of *H. pylori*, an abundant pathogen in the stomach and leading cause of ulcers [10,11]. It has been shown that viscoelasticity is a more crucial factor in controlling the maximum velocity of lyme disease pathogen *B. burgdorferi* through skin than even chemical composition [12]. Viscoelastic properties of mucus have a remarkable impact on the swimming of spermatozoa and sperm-egg encounter rates [13].

Despite the widespread implications of viscoelastic effects on biological processes, research on motile microorganism dynamics in confined environments is largely limited to Newtonian fluids [14–24]. Recently, a large number of studies have considered locomotion in quiescent non-Newtonian fluids at the scale of microswimmers, in experiments, simulations, and theory [25–32], but little is known about the dynamical behavior of swimmers subject to large-scale non-Newtonian flows.

In this Letter, we construct a tractable theoretical framework for individual microorganisms swimming in confined, flowing microbiological environments of non-Newtonian fluids. We study the macroscopic effects of shear-dependent viscosity and viscoelasticity, both in separation and in conjunction, for a weakly viscoelastic fluid. Image systems are introduced, regularizing the hydrodynamic interactions of microswimmers with the walls, and swimmer trajectories are characterized. Shear-dependent viscosity is seen to greatly impact the upstream motion of motile cells, and our analysis shows that the presence of normal stress differences in viscoelastic fluids results in a remarkable upstream migration along the centerline. We provide quantitative measures of the upstream motion and propose a novel sorting mechanism for motile organisms in confined viscoelastic flows.

A single microorganism is modeled as swimming in flowing, incompressible, non-Newtonian fluid within a channel of height $2H$ (Fig. 1). In addition to its swimming velocity $\boldsymbol{v}_s = v_s \boldsymbol{p}_s$ in the direction $\boldsymbol{p}_s$, the motion of the swimming cell of radius a is affected by the background flow $\boldsymbol{v}_f$, hydrodynamic interactions (HIs) with the channel walls $\boldsymbol{v}_{\mathrm{HI}}$, and cross-streamline migration induced by viscoelastic normal stress difference gradients $\boldsymbol{v}_M$. Thus, the evolutions of a microswimmer's position and direction are

$$\dot{\boldsymbol{r}}_s = \boldsymbol{v}_s + \boldsymbol{v}_f + \boldsymbol{v}_{\mathrm{HI}} + \boldsymbol{v}_M, \tag{1}$$

$$\dot{\boldsymbol{p}}_s = \Omega_f \times \boldsymbol{p}_s + \Omega_{\mathrm{HI}} \times \boldsymbol{p}_s, \tag{2}$$

where $\Omega_f = \frac{1}{2}\boldsymbol{\nabla} \times \boldsymbol{v}_f$ and Ω_{HI} denotes the angular velocity due to the HIs with the walls.

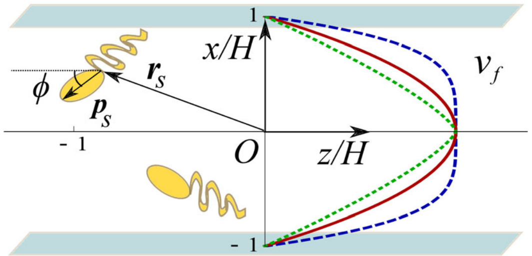

FIG. 1. Schematic of a microswimmer at position $\boldsymbol{r}_s$ and moving with speed v_s in the direction $\boldsymbol{p}_s$ subject to a viscoelastic flow within a microchannel of height $2H$. The Poiseuille flow $\boldsymbol{v}_f$ is shown for shear-thinning (blue, dashed line), Newtonian (red, solid line), and shear-thickening (green, dotted line) fluids.

The translational invariance of Eqs. (1) and (2) along the y and z directions allows us to consider the motion of swimmers in the $y = 0$ plane, and orientation can be represented in cylindrical coordinates as $\boldsymbol{p}_s = -\sin(\phi)\hat{\boldsymbol{e}}_x - \cos(\phi)\hat{\boldsymbol{e}}_z$, where $\phi \in [-\pi, \pi]$ is the angle in the x-z plane. Upstream swimming corresponds to $\phi = 0$ and downstream to $\pm\pi$ (Fig. 1). Consequently, the dynamics of the system can be represented by two coupled equations, $\dot{x} = \dot{x}(x, \phi)$ and $\dot{\phi} = \dot{\phi}(x, \phi)$, and a third uncoupled equation $\dot{z} = \dot{z}(x, \phi)$. We nondimensionalize lengths by half the channel height, H, and velocities by the swimming speed, v_s. Therefore, changes in the swimming speed due to viscoelasticity, as studied in Refs. [25–32], are readily incorporated into this model.

In a Newtonian fluid, this system shows the emergence of swinging and tumbling microswimmer trajectories in Poiseuille flow [16,18]. Upstream-oriented swimmers are rotated by background vorticity so that they oscillate about the centerline [Figs. 2(a) and 2(b); green trajectory]. For large oscillation amplitudes, however, the swimmer runs into the walls [Fig. 2(a); red trajectory]. Hence, HIs with the boundaries must be included [16]. Simply including the far-field force dipole of strength κ and an image system consisting of a superposition of point-force singularities [33] in the HIs produces nonphysical singular flow fields near the walls, unless a physical cutoff length is provided.

We construct a more physical representation by including a source doublet of strength σ in the swimmer's flow and image fields, producing a more accurate near-field flow and regularizing the HIs with the boundaries. This ensures that the swimmer is turned away from the boundaries by the closest distance of approach $h_m = (\sigma/v_s)^{1/3}$, which sets a natural cutoff and gives an effective size. This may be understood to be its hydrodynamic radius, $a_h = (2\sigma/v_s)^{1/3}$ [34], which we expect to be directly proportional to the swimmer size; $a_h \sim a$, and thus $h_m \sim a$. For example, *Volvox* has $\sigma \sim 10^9$ $\mu\text{m}^4/\text{s}$ and $v_s \sim 10^2$ $\mu\text{m/s}$ [35], so that $a_h \sim 270$ μm compared to $a \sim 200$ μm. By including the near-field correction, unphysical swimmer-wall contact is ruled out and the swimmer trajectory runs parallel to the wall with the offset h_m [Fig. 2(b); blue trajectory]. To consistently account for finite-size effects, we also include the Faxén corrections to the flow induced translational, $\boldsymbol{v}_f$, and the angular velocity, $\boldsymbol{\Omega}_f$, of the swimmer [36].

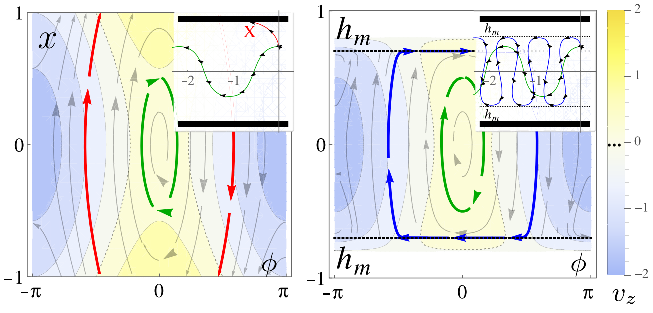

(a) Non-regularised HIs (b) Regularised HIs

FIG. 2. Typical trajectories for swimmer dynamics in a Newtonian Poiseuille flow shown in x-ϕ phase space, and in the x-z plane (insets). The swimmer and maximum flow velocities are $v_s = 1$ and $v_{\max} = 0.75$, and the dipole moment is $\kappa = 0$. (a) Nonregularized HIs, $\sigma = 0$. (b) Regularized HIs with $\sigma = (3/10)^3$, so that $h_m = 3/10$. The background colors indicate the velocity in the z direction.

Non-Newtonian effects modify the background flow and trajectories of microswimmers. Non-Newtonian fluids generally feature two properties that differ from a Newtonian counterpart—namely, shear-dependent viscosity and normal stress differences. Here, shear-thinning and -thickening effects are accounted for via a power-law fluid model $\eta = \eta_0(\dot{\gamma}/\dot{\gamma}_0)^{n-1}$, where $\dot{\gamma}$ is the shear rate, η_0 is the viscosity at the shear rate $\dot{\gamma}_0$, and n is the shear-thinning parameter. The background Poiseuille flow of a power-law fluid is

$$\boldsymbol{v}_f(\boldsymbol{r}) = v_{\max}(1 - (|x|/H)^{(1+n)/n})\hat{\boldsymbol{e}}_z, \tag{3}$$

where $v_{\max}$ is the maximum flow speed. This results in a stronger (weaker) flow near the walls, in shear-thinning (-thickening) fluids compared to a Newtonian fluid with the same $v_{\max}$ (Fig. 1). HIs with the walls remain approximately Newtonian for weakly non-Newtonian fluids since the asymmetric correction for a dipolar swimmer [37,38] decays rapidly as $\sim r^{-3}$ [39,40], which is small compared to the Newtonian contribution and amounts to a negligible correction on the quadrupolar term.

The upstream motion of a swimmer is enhanced in a shear-thickening fluid compared to a shear-thinning counterpart without normal stresses (Fig. 3 and Supplemental Material movie 1 [41]). This is associated with changes in vorticity in the vicinity of the walls. The stronger vorticity of the shear-thinning fluid near the wall results in a more rapid reorientation towards the centerline. Consequently, the swimmer has less time to move upstream.

An initially upstream-oriented swimmer [Fig. 3(a); blue trajectory] in a shear-thinning fluid moves a short distance upstream after the first oscillation about the centerline, whereas the swimmer in the shear-thickening fluid progresses an order of magnitude further. Swimmers initially orientated towards the walls [Fig. 3(a); dashed green trajectories] are carried by the flow, but in a shear-thickening fluid they move further upstream near the walls. Similarly, swimmers initially orientated downstream [Fig. 3(a); dotted red trajectories] experience an enhanced downstream motion in a shear-thinning fluid. This demonstrates that the dynamics in flowing non-Newtonian environments can have a more significant effect on motion than relatively small modifications to the swimming speed in quiescent non-Newtonian fluids [25–32].

If $v_{\max} = v_s$, swimmers oriented directly upstream at the centerline do not progress, while those that oscillate about the centerline experience less counterflow on average and,

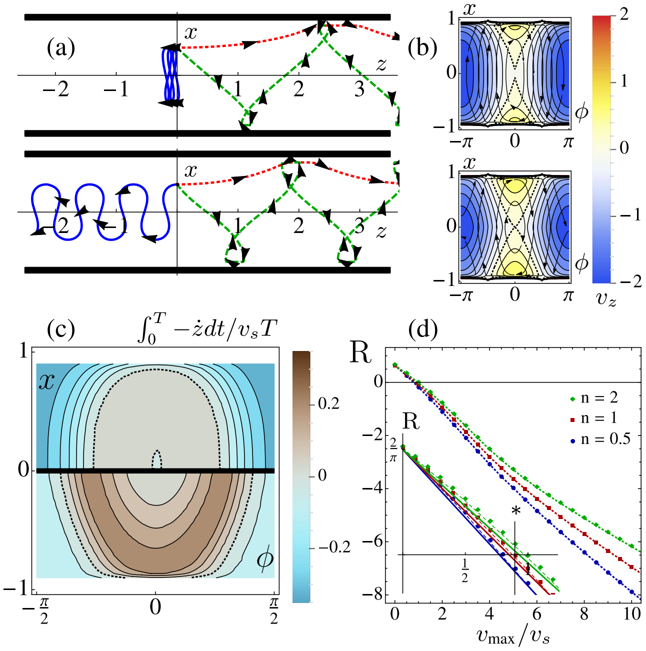

FIG. 3. Swimmer dynamics in Poiseuille flow of a shear-thinning ($n = \frac{1}{2}$) and -thickening fluid ($n = 2$) without normal stresses, shown in the upper and lower halves of subfigures (a)–(c). $v_s = v_{\max} = 1$, $\kappa = 0$, and $\sigma = (1/10)^3$. (a) Trajectories in the x-z plane, with initial position $\boldsymbol{r}_s = (0, 1/2)$ and orientations $\phi = 0$ (blue), $\pi/2$ (green), and π (red). (b) Trajectories in x-ϕ phase space. The background colors indicate the velocity in the z direction. (c) Upstream swimming velocity, $-\dot{z}$, averaged over a large time, for all upstream-oriented initializations in x-ϕ space. (d) Upstream retention ratio, defined by (c) averaged over these initial conditions, as a function of the flow speed. Points show full numerical solutions, dashed lines show theoretical predictions, and solid lines show the limit $v_{\max} \ll v_s$, Eq. (4). The inset focuses on this limit.

therefore, are able to migrate upstream [Figs. 3(b) and 3(c)]. However, if the oscillations about the centerline are too large, the swimmer cannot move upstream. Therefore, the effective upstream motility is not well described by any given trajectory but rather by a retention ratio [42], the ratio of the time-averaged z component of swimmer velocity to the swimming speed, $R = \langle T^{-1} \int_0^T -\dot{z}(t; x_0, \phi_0) dt \rangle / v_s$, where we average over all upstream-oriented trajectories $x_0 \in [-H + h_m, H - h_m]$ and $\phi_0 \in [-\pi/2, \pi/2]$. The upstream retention ratio can be determined numerically [Fig. 3(d); data points] and be approximated analytically. A conserved quantity of motion can be found by integrating $\dot{x}/\dot{\phi}$, giving $\mathcal{C} = 1 + \frac{1}{2} v_{\max} |x|^{(1+n)/n} - v_s \cos\phi$. Hence, the distance traveled along z per oscillation can be computed, $D = \int_{\mathrm{traj}} \dot{z}\, dt$, as well as the period, $T = \int_{\mathrm{traj}} dt$. Dividing these and averaging over the initial conditions gives $R = -\langle D/v_s T \rangle$ [Fig. 3(d); dashed lines]. In the limit of $v_{\max} \ll v_s$, we find the linear relation [Fig. 3(d); the solid lines]

$$R = \frac{2}{\pi} - \frac{2 + 9n + 7n^2}{2 + 10n + 12n^2} \frac{v_{\max}}{v_s}. \tag{4}$$

Hence, the difference in upstream retention ratio for shear-thinning and -thickening fluids grows with increasing flow speed. This determines the crossover between upstream and downstream motion of the majority of swimmers where $R = 0$ [see the inset of Fig. 3(d)]. The slopes change at larger flow speeds, $v_{\max} > 4v_s$, when the tumbling trajectories start to outnumber the oscillating trajectories [16], and the full solution for R must be applied (the dashed lines). In this $v_{\max} \gg v_s$ regime, the difference in upstream retention ratio for shear-thinning and -thickening fluids can be large [Fig. 3(d)]. For $v_{\max} = 10v_s$, the shear thickening ($n = 2$) R value differs by 33% from the shear-thinning ($n = 1/2$) value, which is substantial compared to the 5%–10% change in swimming speed observed in quiescent non-Newtonian fluids [25–32].

The significant modification of upstream retention ratios in non-Newtonian fluids can have important consequences in microbiological flows. For instance, our results suggest that a motile *H. pylori*, swimming with an average velocity of 27 μm/s [11] and subjected to gastric mucosal flow with a similar velocity and $n = 0.5$, would have a 50% reduction in upstream retention ratio than if it were swimming in a Newtonian fluid flow ($n = 1$). Since the velocity of the mucosal flow can vary broadly [43] and n can be as small as ~0.15 [11,43,44], this serves as a conservative example.

In addition to shear-dependent viscosities, many microbiological fluids are characterized by viscoelastic normal stress differences. To describe these, with a power-law viscosity, we employ the second-order fluid model [45] with the stress tensor $S_{ij} = -p\delta_{ij} + \eta(\dot{\gamma}) D_{ij}^{(1)} - \frac{1}{2}\psi_1 D_{ij}^{(2)} + (\psi_1 + \psi_2) D_{ik}^{(1)} D_{kj}^{(1)}$, where ψ_1 and ψ_2 are the first and second normal stress coefficients and $D_{ij}^{(1)}$ and $D_{ij}^{(2)}$ are the Rivlin-Eriksen tensors. The Deborah number is $\boxed{\mathrm{De}} = v_{\max}(\psi_1 - 2\psi_2)/(\eta H) \ll 1$. The normal stress coefficients characterize the fluid elasticity. These terms do not alter the undisturbed flow profile of Eq. (3) in the absence of swimmers. However, the disturbance flow around a finite-size swimmer in combination with nonuniform shear across the channel results in a normal stress imbalance that causes a lateral migration across streamlines. Normal stress-induced migration of passive, inertialess particles in pressure-driven flow is well documented [46–54]. To determine the migration velocity we use Chan and Leal's solution for general quadratic flow [47] by expanding the background flow profile [Eq. (3)] about the swimmer position, as reported previously [53]. In our system, the migration velocity is then

$$\boldsymbol{v}_M = -\psi_n \left(\frac{|x|}{H}\right)^{(3-2n)/n} \hat{\boldsymbol{e}}_x, \tag{5}$$

where $\psi_n = \psi_s a^2 v_{\max}^{3-n} \gamma_0^{n-1} f(n)/\eta_0 H^{4-n}$, $f(n) = 5(1+n)^{3-n}/36n^{4-n}$, and $\psi_s = \psi_1 - 2\psi_2$. The function ψ_n encapsulates both the non-Newtonian effects of normal stress differences and shear-dependent viscosity. A viscoelastic torque Ω_M is not included in Eq. (2) [53] because this term is insignificant compared to the vorticity when $\mathrm{De} \ll 1$ and, by symmetry of the swimmer, does not lead to preferred orientations.

In both the shear-thinning and -thickening cases with normal stresses, the swimmer is driven to the centerline, and the coupling between motility and streamline migration rotates the swimmer to move upstream along the centerline [Fig. 4(a)]. Unlike in a Newtonian fluid, the oscillations about the centerline are now damped in amplitude as the phase space origin ($x = \phi = 0$) is a stable, attractive spiral [Fig. 4(b)]. The attraction is stronger for shear-thinning than shear-thickening fluids.

We analyze this effect by linearizing the equations of motion [Eqs. (1) and (2)] about the origin so that $(\dot{\phi}, \dot{x})^T = \boldsymbol{M}(\phi, x)^T$, where

$$\boldsymbol{M} = \begin{pmatrix} -\frac{3\kappa}{4} & v_f + \frac{3\sigma}{2} \\ -v_s + \frac{\sigma}{4} + \frac{3\nu}{2} & \frac{3\kappa}{2} - \psi_n \end{pmatrix}. \tag{6}$$

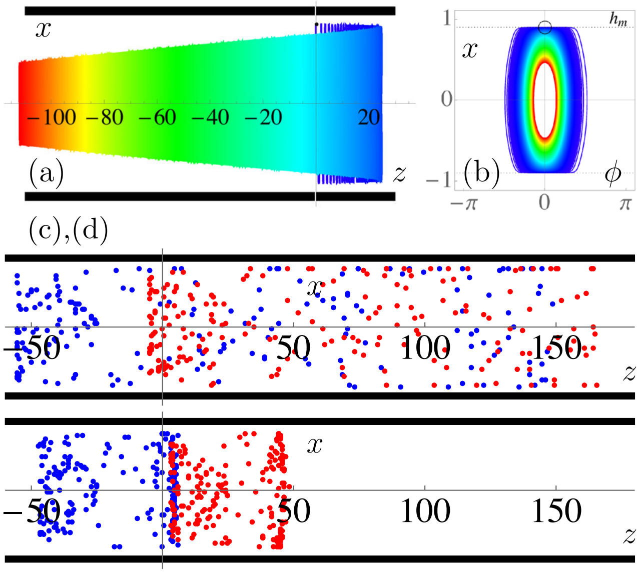

FIG. 4. Swimmer dynamics in Poiseuille flow of a shear-thinning viscoelastic fluid with $\mathrm{De} = 0.1$, $n = 0.8$, and $v_{\max} = 1 v_s$. The swimmer parameters are $a = 0.1$, $v_s = 1$, $\kappa = 0$, and $\sigma = 10^{-3}$. (a) Oscillating trajectory in the x-z plane with initial position $\boldsymbol{r}_s = (0, 0.9)$ and orientations $\phi = 0$. (b) Corresponding trajectory in x-ϕ phase space. Colors indicate time progressing, from $t = 0$ (blue) to $t = 1000$ (red). The swimmers are focused towards the centerline and are reoriented to move upstream. (c),(d) Two ensembles of swimmers, with $v_s = 1.1$ (blue) and $v_s = 0.9$ (red), are released from a random x position and orientation in the channel at $z = 0$. In a Newtonian fluid (c), the swimmers are dispersed, but in a viscoelastic fluid (d) they remain clustered and are sorted according to swimming speed over time.

In $\boldsymbol{M}$, ψ_n and the dipolar HI terms are responsible for the spiral. Away from the walls, viscoelasticity dominates over HI effects and the eigenvalues of $\boldsymbol{M}$ without HIs are found to be $\lambda_\pm = \frac{1}{2}(-\psi_n \pm \sqrt{\psi_n^2 - 4 v_{\max} v_s})$. Hence, the origin is a stable fixed point if $\psi_n^2 > 4 v_{\max} v_s$ with two real negative (attractive) eigenvalues. Otherwise, the origin is a stable spiral with complex eigenvalues and negative real parts, meaning that swimmers perform damped oscillations about the centerline, as verified in Figs. 4(a) and 4(b). Because the function $f(n)$ decreases monotonically with n, ψ_n is larger for shear-thinning fluids, and therefore the attraction towards the centerline is greater.

Though more pronounced in shear-thinning than shear-thickening flows, swimmers in flowing viscoelastic fluids tend to move upstream along the centerline after some time, regardless of initial position or upstream orientation. This allows for a sorting mechanism to select swimmers with a given swimming speed larger than the tunable Poiseuille flow, as demonstrated in Figs. 4(c) and 4(d), where distributions of swimmers with different self-propulsion velocities are initially introduced at random positions and orientations in the channel in Newtonian and shear-thinning viscoelastic fluids. Unlike the Newtonian fluid, swimmers with larger motility are separated by moving upstream in the viscoelastic fluid (see the Supplemental Material movies 2 and 3 in Ref. [41]). It is worth noting that we expect this sorting mechanism to be robust against translational and orientational noise since small amounts of noise will keep the oscillation size nonzero, enhancing the upstream retention ratio and hence the sorting.

To summarize, unlike the prevalent boundary accumulation in quiescent Newtonian fluids, swimmers' trajectories show oscillatory motion about the centerline. Average migration against Poiseuille flows is enhanced (reduced) in shear-thickening (-thinning) fluids compared to simple Newtonian fluids. It is not necessary that the non-Newtonian nature of these fluids be appreciable on the microscale since altered trajectories arise from differences in vorticity at macroscopic scales. This constitutes a substantial change to the effective upstream motility, that is comparable to or greater than observed changes in motility due to microscopic effects on swimming in quiescent non-Newtonian fluids [25–32,55,56]. The oscillations are damped towards the centerline in the presence of viscoelastic normal stress differences resulting in direct upstream migration. This offers a sorting mechanism to differentiate motile microorganisms according to speed.

We gratefully thank Andreas Zöttl for his helpful comments on the manuscript. This work was funded through ERC Advanced Grant No. 291234 MiCE, and we acknowledge EMBO for support to T. N. S. (Grant No. ALTF181-2013).

---

[*] mathijssen@physics.ox.ac.uk

[1] K. Miki and D. E. Clapham, Curr. Biol. 23, 443 (2013).

[2] E. A. Simone, T. D. Dziubla, and V. R. Muzykantov, Expert Opin. Drug Delivery **5**, 1283 (2008).

[3] M. Brown and C. Wittwer, Clin. Chem. (Washington, DC) **46**, 1221 (2000).

[4] S. Berger and L. Jou, Annu. Rev. Fluid Mech. **32**, 347 (2000).

[5] S. Hwang, M. Litt, and W. Forsman, Rheol. Acta **8**, 438 (1969).

[6] A. Gilboa and A. Silberberg, Biorheology **13**, 59 (1976).

[7] T. J. Moriarty, M. U. Norman, P. Colarusso, T. Bankhead, P. Kubes, and G. Chaconas, PLoS Pathogens **4**, e1000090 (2008).

[8] M. J. Hickey and P. Kubes, Nat. Rev. Immunol. **9**, 364 (2009).

[9] J. D. Radolf, M. J. Caimano, B. Stevenson, and L. T. Hu, Nat. Rev. Microbiol. **10**, 87 (2012).

[10] C. Montecucco and R. Rappuoli, Nat. Rev. Mol. Cell Biol. **2**, 457 (2001).

[11] J. P. Celli, B. S. Turner, N. H. Afdhal, S. Keates, I. Ghiran, C. P. Kelly, R. H. Ewoldt, G. H. McKinley, P. So, S. Erramilli, and R. Bansil, Proc. Natl. Acad. Sci. U.S.A. **106**, 14321 (2009).

[12] R. B. Kimsey and A. Spielman, J. Infect. Dis. **162**, 1205 (1990).

[13] J. A. Riffell and R. K. Zimmer, J. Exp. Biol. **210**, 3644 (2007).

[14] A. Karimi, S. Yazdi, and A. Ardekani, Biomicrofluidics **7**, 021501 (2013).

[15] S. Uppaluri, N. Heddergott, E. Stellamanns, S. Herminghaus, A. Zöttl, H. Stark, M. Engstler, and T. Pfohl, Biophys J. **103**, 1162 (2012).

[16] A. Zöttl and H. Stark, Phys. Rev. Lett. **108**, 218104 (2012).

[17] A. Costanzo, R. Di Leonardo, G. Ruocco, and L. Angelani, J. Phys. Condens. Matter **24**, 065101 (2012).

[18] A. Zöttl and H. Stark, Eur. Phys. J. E **36**, 4 (2013).

[19] N. Figueroa-Morales, G. Leonardo Miño, A. Rivera, R. Caballero, E. Clément, E. Altshulerb, and A. Lindner, Soft Matter **11**, 6284 (2015).

[20] R. Ledesma-Aguilar and J. M. Yeomans, Phys. Rev. Lett. **111**, 138101 (2013).

[21] R. Rusconi, J. S. Guasto, and R. Stocker, Nat. Phys. **10**, 212 (2014).

[22] S. Chilukuri, C. H. Collins, and P. T. Underhill, J. Phys. Condens. Matter **26**, 115101 (2014).

[23] A. Costanzo, J. Elgeti, T. Auth, G. Gompper, and M. Ripoll, Europhys. Lett. **107**, 36003 (2014).

[24] C. K. Tung, F. Ardon, A. Roy, D. L. Koch, S. S. Suarez, and M. Wu, Phys. Rev. Lett. **114**, 108102 (2015).

[25] B. Liu, T. R. Powers, and K. S. Breuer, Proc. Natl. Acad. Sci. U.S.A. **108**, 19516 (2011).

[26] D. Gagnon, N. Keim, and P. Arratia, J. Fluid Mech. **758**, R3 (2014).

[27] Y. Gao, M. Neubauer, A. Yang, N. Johnson, M. Morse, G. Li, and J. X. Tang, BMC Microbiol. **14**, 322 (2014).

[28] V. A. Martinez, J. Schwarz-Linek, M. Reufer, L. G. Wilson, A. N. Morozov, and W. C. Poon, Proc. Natl. Acad. Sci. U.S.A. **111**, 17771 (2014).

[29] E. Lauga, Phys. Fluids **19**, 083104 (2007).

[30] H. C. Fu, V. B. Shenoy, and T. R. Powers, Europhys. Lett. **91**, 24002 (2010).

[31] J. Teran, L. Fauci, and M. Shelley, Phys. Rev. Lett. **104**, 038101 (2010).

[32] S. E. Spagnolie, B. Liu, and T. R. Powers, Phys. Rev. Lett. **111**, 068101 (2013).

[33] S. E. Spagnolie and E. Lauga, J. Fluid Mech. **700**, 105 (2012).

[34] A. J. Mathijssen, D. O. Pushkin, and J. M. Yeomans, J. Fluid Mech. **773**, 498 (2015).

[35] K. Drescher, R. E. Goldstein, N. Michel, M. Polin, and I. Tuval, Phys. Rev. Lett. **105**, 168101 (2010).

[36] S. Kim and S. Karilla, *Microhydrodynamics*, Butterworth Series of Chemical Engineering (Dover, New York, 1991).

[37] O. S. Pak, L. Zhu, L. Brandt, and E. Lauga, Phys. Fluids **24**, 103102 (2012).

[38] L. Zhu, E. Lauga, and L. Brandt, Phys. Fluids **24**, 051902 (2012).

[39] A. Acharya, R. Mashelkar, and J. Ulbrecht, Rheol. Acta **15**, 454 (1976).

[40] R. J. Phillips and L. Talini, J. Non-Newtonian Fluid Mech. **147**, 175 (2007).

[41] See Supplemental Material at http://link.aps.org/supplemental/10.1103/PhysRevLett.116.028104 for movies.

[42] K. G. Wahlund, J. Chromatogr. A **1287**, 97 (2013).

[43] N. Sato, S. Kawano, S. Tsuji, T. Ogihara, and S. Yamada, Scand. J. Gastroenterol. **30**, 14 (1995).

[44] A. Rösler, G. W. Vandermeulen, and H. M. Klok, Adv. Drug Delivery Rev. **64**, 270 (2012).

[45] R. B. Bird, R. C. Armstrong, O. Hassager, and C. F. Curtiss, *Dynamics of Polymeric Liquids*, Vol. 1 (Wiley, New York, 1977).

[46] B. Ho and L. Leal, J. Fluid Mech. **76**, 783 (1976).

[47] P.-H. Chan and L. Leal, J. Fluid Mech. **82**, 549 (1977).

[48] L. Leal, Annu. Rev. Fluid Mech. **12**, 435 (1980).

[49] A. M. Leshansky, A. Bransky, N. Korin, and U. Dinnar, Phys. Rev. Lett. **98**, 234501 (2007).

[50] G. d'Avino, P. L. Maffettone, F. Greco, and M. Hulsen, J. Non-Newtonian Fluid Mech. **165**, 466 (2010).

[51] M. M. Villone, G. D'Avino, M. A. Hulsen, F. Greco, and P. L. Maffettone, Comput. Fluids **42**, 82 (2011).

[52] M. Villone, G. D'Avino, M. Hulsen, F. Greco, and P. L. Maffettone, J. Non-Newtonian Fluid Mech. **166**, 1396 (2011).

[53] A. M. Ardekani and E. Gore, Phys. Rev. E **85**, 056309 (2012).

[54] G. D'Avino and P. Maffettone, J. Non-Newtonian Fluid Mech. **215**, 80 (2015).

[55] G. Li and A. M. Ardekani, J. Fluid Mech. **784**, R5 (2015).

[56] C. Datt, L. Zhu, G. J. Elfring and O. S. Pak, J. Fluid Mech. **784**, R4 (2015).